Materials Science and Engineering C 58 (2016) 666–674

Contents lists available at ScienceDirect

Materials Science and Engineering C

journal homepage: www.elsevier.com/locate/msec

Fabrication of graphene/gold-modified screen-printed electrode for detection of carcinoembryonic antigen

K.F. Chan [a], H.N. Lim [a,*], N. Shams [a], S. Jayabal [b], A. Pandikumar [b], N.M. Huang [b]

[a] Department of Chemistry, Faculty of Science, Universiti Putra Malaysia, UPM Serdang, 43400 Selangor, Malaysia
[b] Low Dimensional Materials Research Centre (LDMRC), Physics Department, Faculty of Science, University of Malaya, 50603 Kuala Lumpur, Malaysia

ARTICLE INFO

Article history:
Received 30 June 2015
Received in revised form 21 August 2015
Accepted 3 September 2015
Available online 7 September 2015

Keywords:
Biosensor
Electrochemistry
Gold nanoparticles
Graphene
Screen-printed electrode

ABSTRACT

Immunosensors based on gold nanoparticles and reduced graphene oxide (AuNPs/rGO)-modified screen-printed electrodes (SPEs) were successfully synthesized using an electrochemical deposition method. The modified SPEs were characterized using a field emission scanning electron microscope (FESEM) and Raman spectroscopy to analyze the morphology and composition of AuNPs and rGO. Both the FESEM and Raman spectroscopy revealed that the AuNPs were successfully anchored on the thin film of rGO deposited on the surface of the SPEs. Characterization with a ferri–ferrocyanide couple [$Fe(CN)_6^{3-/4-}$] showed that the electron transfer kinetic between the analyte and electrode was enhanced after the modification with the AuNPs/rGO composite on the electrode surface, in addition to increasing the effective surface area of the electrode. The modified SPE was immobilized with a sandwich type immunosensor to mimic the ELISA (enzyme-linked immunosorbent assay) immunoassay. The modified SPE that was fortified with the sandwich type immunosensor exhibited double electrochemical responses in the detection of carcinoembryonic antigen (CEA), with linear ranges of 0.5–50 ng/mL and 250–2000 ng/mL and limits of detection of 0.28 ng/mL and 181.5 ng/mL, respectively.

1. Introduction

Cancer diagnosis and treatment is gaining great attention globally because of the prevalence, high fatality rate, and possible recurrence of the disease after treatment [1]. Early cancer detection methods include screening methods such as a Papanicolau test for cervical cancer and mammography for breast cancer in women, prostate-specific antigen (PSA) level detection in a blood sample for men to detect prostate cancer, enzyme-linked immunosorbent assay (ELISA), radiation immunological assays (RIAs), occult blood detection for colon cancer, and instrumental approaches such as endoscopy, CT scans, X-ray, ultrasound imaging, MRI, time-resolved fluorescence, and chemiluminescence [2]. An increased level of a tumor marker in human serum is a reliable symptom associated with cancer patients. Thus, the determination of a tumor marker plays an important role in the early diagnosis of cancer [3]. In clinical assays, the detection methods for tumor markers, which include RIAs, time-resolved fluorescence, and chemiluminescence, have the disadvantages of being environmentally unfriendly, time-consuming, and difficult to automate, as well as having poor precision. The costs of specific instruments and reagents also limit their wide application in clinical laboratories. Hence, there is a need to develop immunosensors that are low-cost and effective, with real-time control [4].

Immunosensors have been known as a core development in the immunochemical field in clinical diagnosis because they combine the advantages of sensors, like high sensitivity, with high specific immune reactions [5]. The remarkable simultaneous monitoring of immunoreactions of immunosensors renders a dynamic analysis of immunoreactions possible [3]. There are five types of immunosensor detection devices: electrochemical (amperometric, potentiometric, capacitive, or impedimetric), optical (fluorescence, luminescence, or refractive index), microgravimetric, thermometric, and immunosensors coupled with other techniques such as flow injection analysis and capillary electrophoresis [6]. Electrochemical devices have traditionally received the major share of the attention in biosensor development [7]. Among the immunosensor devices, an electrochemical immunoassay has a low detection limit, requires a small analyte volume, simple instrumentation, and minimal manipulation, and the system can be easily miniaturized and integrated in biochips [8]. Apart from that, the advantages of high sensitivity, specificity, simplicity, and inherent miniaturization of electrochemical immunosensors make them a significant rival of the most advanced optical methods [9]. Although an electrochemical ELISA requires a suitable electrode to contact the analyte solution, many groups have been focusing on the potential miniaturization of an ELISA system in combination with various electrochemical methods [10]. Miniaturized systems offer many potential advantages over conventional assay platforms, including small sample volumes, low cost, short assay time, high throughput, and automation [11].

* Corresponding author.
E-mail address: janetlimhn@gmail.com (H.N. Lim).

http://dx.doi.org/10.1016/j.msec.2015.09.010
0928-4931/

Screen-printing technology, which has been adopted for microelectronics, is significantly used to fabricate electrodes for disposable electrochemical biosensors [12]. A screen-printed electrode (SPE) is simple, versatile, low cost, portable, easily operated, reliable, small sized, and capable of mass production. Therefore, it is applied widely in the electroanalytical chemistry field [13]. Furthermore, a screen-printed electrode avoids the cleaning process, unlike conventional electrodes such as a glassy carbon electrode (GCE) [14]. An SPE avoids the disadvantages of conventional three- and two-electrode systems, which need frequent re-calibration and are unstable and unsuitable for on-site analysis, because they can take several hours to complete. In addition, these must be performed by trained personnel and require numerous separations and washing steps. These drawbacks of conventional electrode systems make them less capable than screen-printed electrodes.

There have been numerous studies and developments in nanotechnology and the application of nanomaterials to the detection of cancer at an early stage. The unique physical, optical, and electrical properties of nanomaterials make them useful in immunosensing. Quantum dots, gold nanoparticles, magnetic nanoparticles, carbon nanotubes, gold nanowires, and many other materials are developed and modified for immunosensors to achieve a wider detection range and lower detection limit for biomarkers [2]. Gold nanoparticles are among the nanoparticles that have been widely used in analytical and biomedical areas because of their speed and ease of use in chemical synthesis, their narrow size distribution, and their convenient labeling of biomolecules [15]. Reduced graphene oxide (rGO) contains hydroxyl (–OH) and carboxylate (–COOH) groups in the structure, which enables interaction with metal nanoparticles to produce a metal nanoparticle–graphene based electrochemical sensor [16]. Insertion of metal nanoparticles prevents graphene layers from stacking to form graphite multi-layered structure [17]. Nanomaterials can be fabricated on an electrode surface through chemical reduction from an aqueous solution of chlorometallate anions, electrochemical deposition, and metal-vapor synthesis. Electrochemical-metal deposition is a convenient and fast method to prepare metal nanoparticles on large areas of conductive electrodes [18]. Green synthesis approach is commonly used to decorate rGO with Au, Pt and Ag nanoparticles to achieve enhanced mechanical, electrical and thermal properties [19].

In the present work, we developed an immunosensor using AuNPs/rGO-modified SPEs through the in-situ electrodeposition of graphene and the reduction of gold cation (Au^{3+}). After the modification of the SPE, a primary antibody, secondary antibody, and carcinoembryonic antigen (CEA) were immobilized on the electrode surface. The modified SPE was characterized using cyclic voltammetry (CV), a field emission scanning electron microscope (FESEM), and a Raman spectrometer. This work realized a convenient, low-cost, and one-step method for fabricating a disposable immunosensor.

2. Experimental

2.1. Chemicals and reagents

Graphite flakes were obtained from Ashbury Inc. (NJ, USA). Sodium dihydrogen phosphate monohydrate ($NaH_2PO_4 \cdot H_2O$, 99%), and disodium hydrogen phosphate dihydrate ($Na_2HPO_4 \cdot 2H_2O$, 99.5%) were purchased from Merck, Germany. Hydrogen tetrachloroaurate (III) trihydrate (ACS, 99.99%) was purchased from abcr GmbH & Co. KG, Germany. Hydrogen chloride (HCl, 37%) and bovine serum albumin (BSA, 96%) were obtained from Sigma-Aldrich. Hydrogen peroxide (H_2O_2, 35%) was purchased from Systerm, Malaysia. A primary antibody (mouse monoclonal, 2.000 mg/mL), carcinoembryonic antigen (CEA, 2.000 mg/mL), secondary antibody (rabbit polyclonal, 2.000 mg/mL), and secondary antibody labeled HRP (goat polyclonal — HRP, 0.500 mg/mL) were obtained from Abcam, USA. SPEs were purchased from DS Dropsens, Spain.

2.2. Synthesis of AuNPs–rGO-modified SPE

Graphene oxide (GO) was synthesized with Hummer's method [20]. First, 1.22 mL of 8.2 g/L synthesized GO was added into a 10 mL volumetric flask. Then, 1.5 mL of 1.0 mM $HAuCl_4$ solution was added into the volumetric flask. The volumetric flask was diluted with 0.1 M (pH 9.2) phosphate buffer solution (PBS). The final solution had a GO concentration of 1.0 mg/mL. After that, the solution was sonicated at a high rate for around 30 s. A bare SPE was washed with ethanol and deionized water. Then, 5 μL of the as-prepared solution was drop casted on the SPE and it was allowed to dry overnight at 25 °C. The SPE was then electrodeposited using a CV potentiostat at potentials from 0 V to −1.5 V in a 0.1 M KCl solution in order to simultaneously reduce the GO to rGO and the Au^{3+} ions to AuNPs nanocomposite. The modified SPE was denoted as AuNPs/rGO-3. A 0.5 mg/mL concentration of GO/AuNPs solution was prepared by repeating the steps, except 0.61 mL of GO was added. This modified SPE was labeled as AuNPs/rGO-2. Another 0.1 mg/mL concentration of GO/AuNPs solution was prepared by diluting 1 mL of the 1.0 mg/mL GO/AuNPs solution in a 10 mL volumetric flask with 0.1 M PBS. This modified SPE was named as AuNPs/rGO-1.

2.3. Immobilization of antibody

The immobilization process of immunoassay was based on the previous work [21]. The modified SPE was dipped in a solution containing 1 mL of N-hydroxysulfosuccinimide (NHS) and 2 mL of 1-ethyl-3-(3-dimethylaminopropyl)-carbodiimide (EDC), which acted as a cross-linker between the primary antibody and AuNPs/rGO nanocomposite. The modified SPE was incubated with the primary antibody (captured antibody) for 2 h at 25 °C. After that, the modified SPE was washed twice with 0.1 M PBS. The modified SPE was blocked with 1% BSA for 2 h at 25 °C. A diluted CEA solution was added to the modified SPE and incubated for 2 h at room temperature. Again, the modified SPE was washed twice with PBS 0.1 M. The modified SPE was incubated with secondary antibody (detection antibody) for 2 h at room temperature. The modified SPE was washed twice with PBS 0.1 M. The modified SPE was incubated with the HRP for 2 h at room temperature. The modified SPE was washed twice with 0.1 M PBS. H_2O_2 was added to the modified SPE in 0.1 M PBS solution, and the signal produced by the enzyme–substrate reaction was measured.

2.4. Characterizations

The morphology and microstructure of the modified SPEs were characterized using the field emission scanning electron microscope (FESEM: FEI Quanta 400F), and a Raman spectrometer (Renishaw in-Via Raman microscope using laser excitation at $\lambda = 514$ nm).

3. Results and discussions

3.1. Morphology and microstructure of AuNPs/rGO modified SPE

Fig. 1 shows the FESEM images of the rGO-modified SPE, AuNPs-modified SPE, and AuNPs/rGO-modified SPE. The morphology of the graphene deposited on the carbon electrode revealed a layer with a typical crumpled and wrinkled structure coating the surface of the carbon electrode [22]. The initially deposited AuNPs acted as nucleation centers for the further reduction of Au^{3+} ions, and hence the size of the AuNPs increased. On the other hand, the AuNPs on the rGO film were not aggregated because of the presence of oxygen functional groups [23]. AuNPs with an average size of 143.77 nm were formed by the electrochemical reduction. The AuNPs were anchored on the graphene film in a well distributed manner. The presence of AuNPs on the graphene film was also supported by a small peak for the Au element shown in the EDX spectrum.

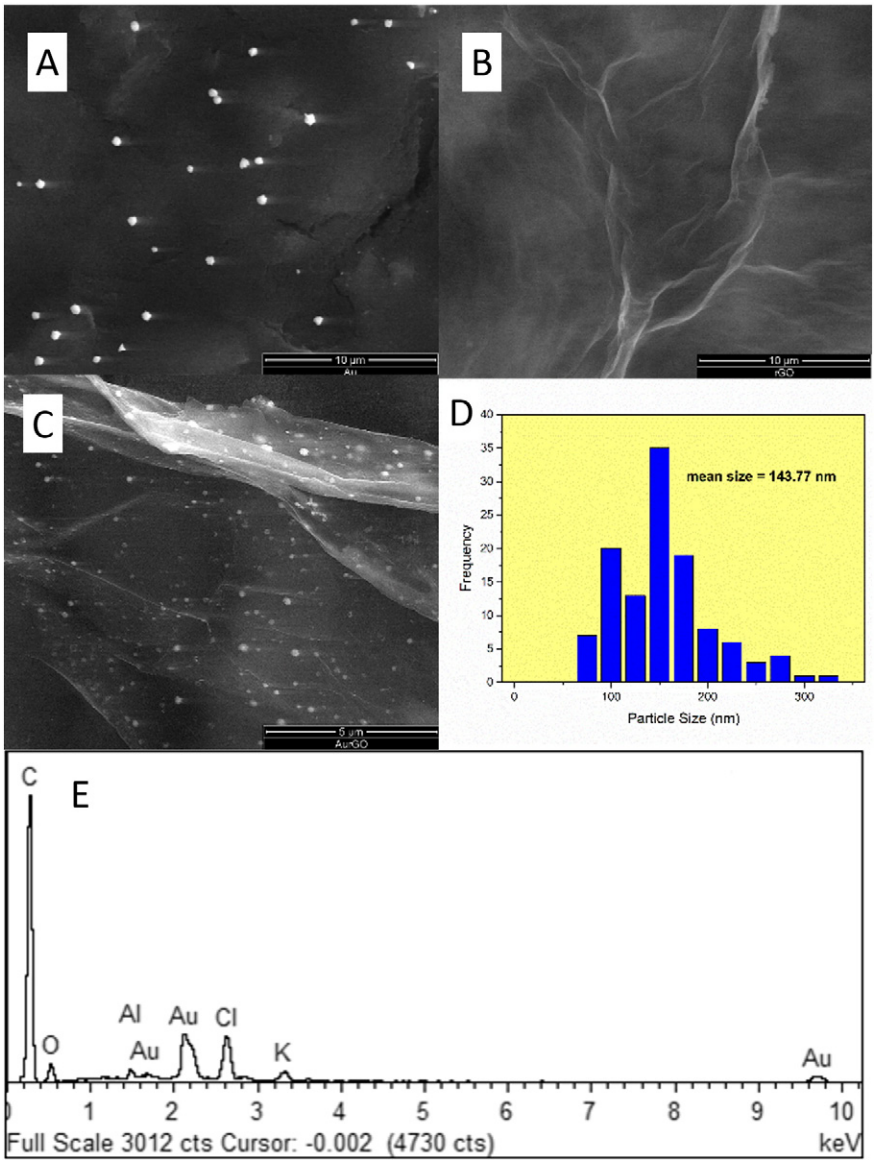

Fig. 1. (A) FESEM image of AuNPs-modified SPE, (B) rGO-modified SPE and (C) AuNPs/rGO-modified SPE. (D) Size distribution graph and (E) EDX of AuNPs/rGO-modified SPE.

The Raman spectra of the graphene–metal nanoparticle composites show the characteristic spectra at different locations (Fig. 2). The Raman spectrum of graphene exhibits the characteristic D-band

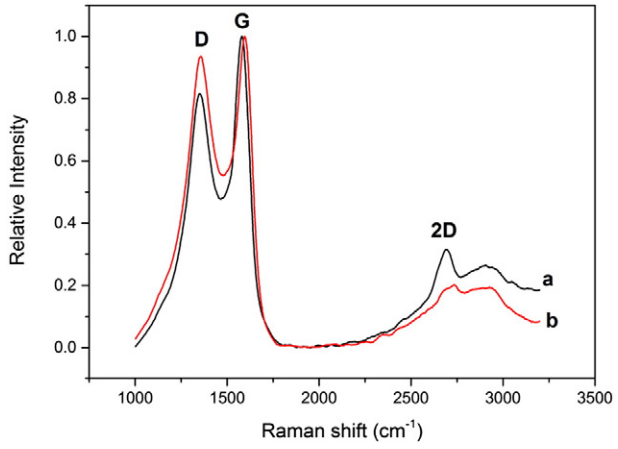

Fig. 2. Raman spectra of (a) AuNPs/rGO-1 (b) rGO-modified SPE.

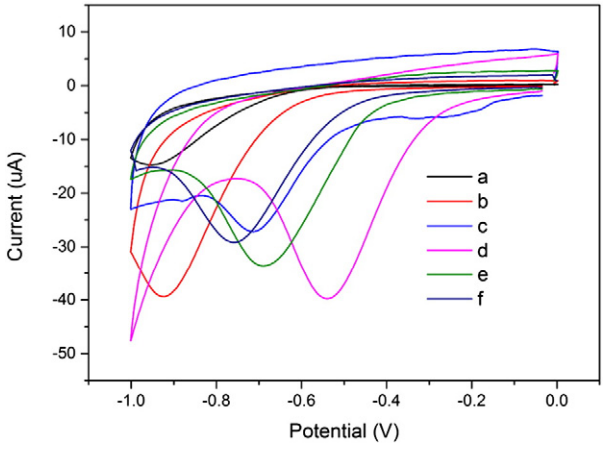

Fig. 3. Cyclic voltammogram for bare SPE (a), AuNPs-modified SPE (b), rGO-modified SPE (c), AuNPs/rGO-1 (d), AuNPs/rGO-2 (e) and AuNPs/rGO-3 (f) in 0.1 M PBS (pH 7.4). The scan rate was 60 mVs^{-1}.

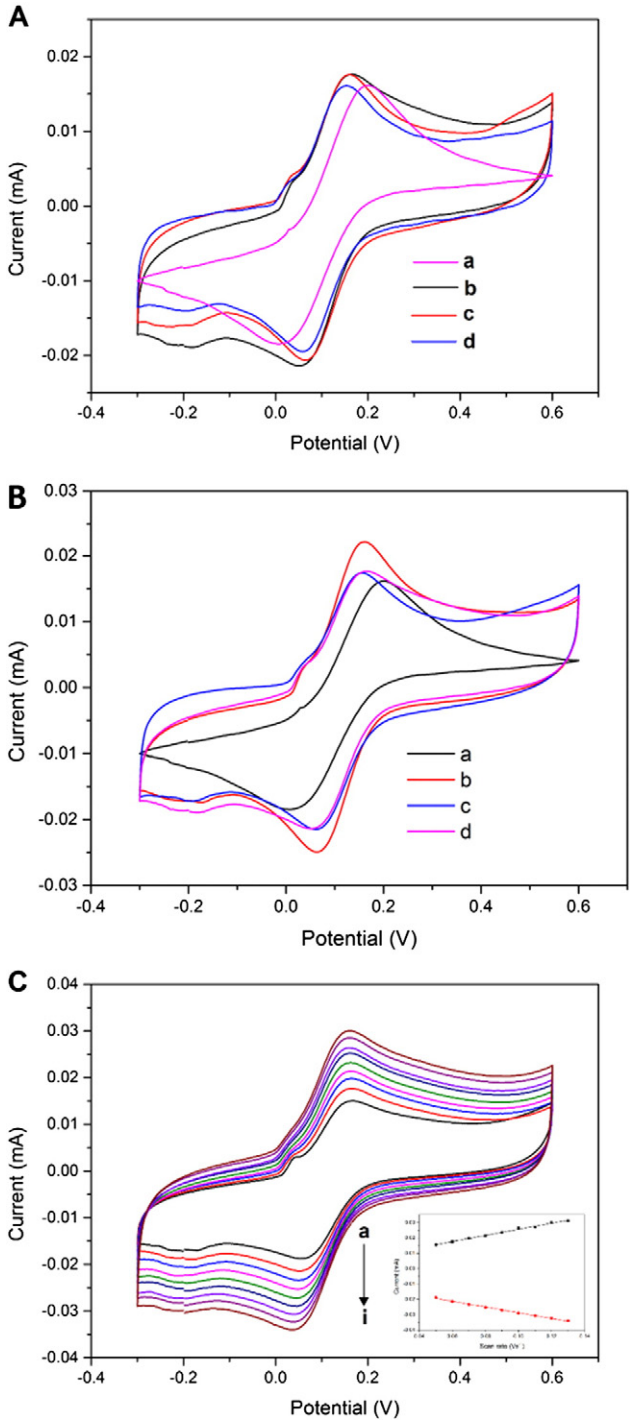

Fig. 4. (A) Cyclic voltammogram of bare SPE (a), AuNPs/rGO-1 (b), AuNPs/rGO-2 (c) and AuNPs/rGO-3 (d) in 0.1 M KCl solution containing 1.0 mM $Fe(CN)_6^{3-/4-}$.The scan rate was 60 mVs^{-1}. (B) Cyclic voltammogram of bare SPE (a), AuNPs-modified SPE (b), rGO-modified SPE (c) and AuNPs/rGO-1 (d). The scan rate was 60 mVs^{-1}. (C) Cyclic voltammogram of AuNPs/rGO-1 in 0.1 M KCl solution containing 1.0 mM $Fe(CN)_6^{3-/4-}$. The scan rate was from 50 mVs^{-1} to 130 mVs^{-1} (a to i). Inset is linear graph of peak current ($I_p/\mu A$) vs square root of scan rate [$v^{1/2}/(Vs^{-1})^{1/2}$].

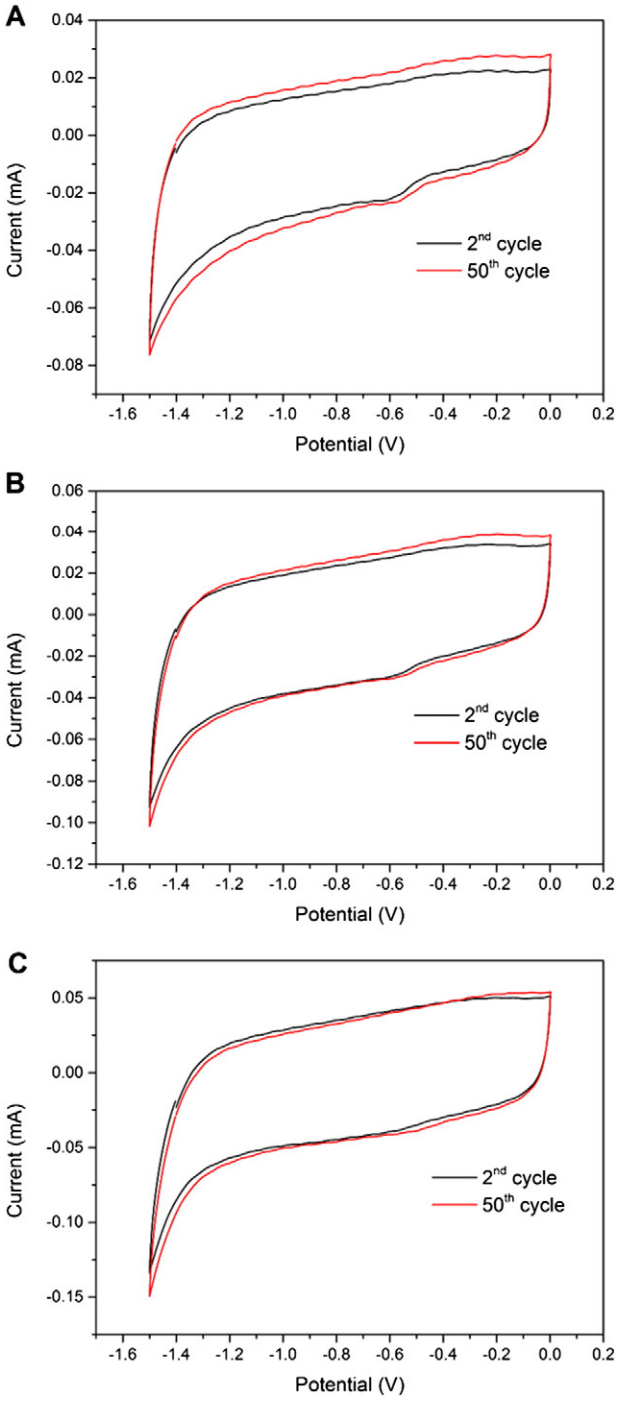

Fig. 5. CV for 2nd and 50th cycle of (A) AuNPs/rGO-1 (B) AuNPs/rGO-2 and (C) AuNPs/rGO-3 in 0.1 M PBS. The scan rate was 60 mVs^{-1}.

(1320 cm^{-1}), G-band (1570 cm^{-1}), D′-band (1600 cm^{-1}), and 2D-band (2635 cm^{-1}). The D and D′-bands are defect-induced features and are absent in defect-free samples. The G-band corresponds to the E_{2g} mode of graphite and arises from the vibration of sp^2-bonded carbon atoms. The 2D-band originates from second-order double-resonant Raman scattering and varies with the number of layers. The intensity of the 2D-band is sensitive to the doping of graphene by holes or electrons [24]. Upon modification of AuNPs on rGO layer, there is a decrease in the D-band frequency by 8 cm^{-1} and the G-band by 27 cm^{-1}, indicating the deposition of AuNPs on the rGO sheet. The intensity of the D-band relative to that of the G-band (I_D/I_G ratio) decreases after the modification of the AuNPs/rGO nanocomposite from 0.96 to 0.81. However, the intensity of the 2D-band relative to that of G-band increases. The decrease in the I_D/I_G intensity was due to the aggregation of AuNPs on the rGO matrices and an increase in the number of graphitic domains, but with a smaller size, which led to the second amorphization stage beyond the critical defect density, where the cluster size (La) of sp^2 was smaller than 2 nm [25–27]. Furthermore, the emergence of the 2D-band (curve a) indicates that the layer of the

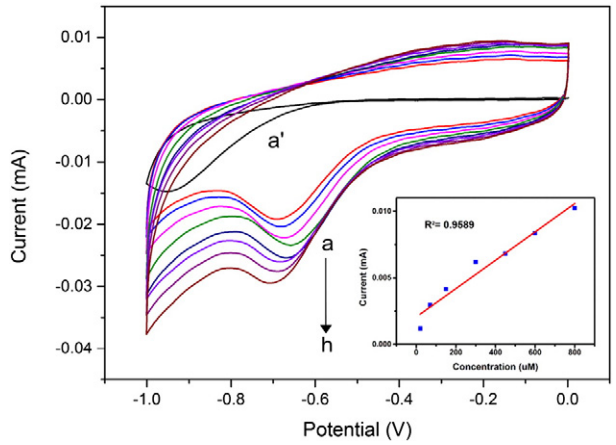

Fig. 6. Cyclic voltammogram of bare SPE (a′) and AuNPs/rGO-1 in 0.1 M pH 7.4 PBS in the presence of 0 μM (a), 20 μM (b), 70 μM (c), 150 μM (d), 300 μM (e), 450 μM (f), 600 μM (g) and 800 μM (h) H_2O_2. The scan rate was 60 mVs^{-1}. Inset is calibration curve of AuNPs/rGO-1 for the detection of H_2O_2.

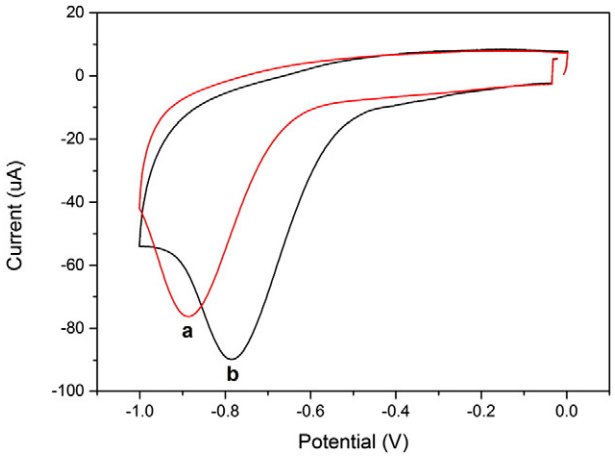

Fig. 8. Cyclic voltammogram of AuNPs/rGO-1 (a) and immunosensor after incubation of 10 ng/mL CEA (b) in 0.1 M PBS (pH 7.4) containing 5 μM H_2O_2. The scan rate was 60 mVs^{-1}.

rGO sheet has multiplied after the doping of AuNPs, which is accompanied by a decrease in the I_D/I_G intensity [28]. The AuNPs and rGO interaction is covalent, and this interaction affects the lattice constant and electronic properties [25]. Hence, the electrodeposition of AuNPs might affect the amount of crystal defects and the properties in the rGO layer compared to that in bare rGO.

3.2. Electrochemical properties of AuNPs/rGO modified SPE

The electrochemical responses of AuNPs/rGO-1, AuNPs/rGO-2, AuNPs/rGO-3, the rGO-modified SPE and the AuNPs-modified SPE were characterized using CV in 0.1 M PBS (pH 7.4), as shown in Fig. 3. The bare SPE was also studied under the same conditions for comparison (curve a). Compared to the AuNPs/rGO-modified SPEs, the bare electrode exhibited a small reduction peak at −0.95 V, indicating that it lacked capability as a redox probe. The rGO-modified SPE showed a slightly higher reduction peak at −0.7 V, with a positive shift (curve b). In the presence of the AuNPs/rGO nanocomposite, significant reduction peaks were shown at −0.54 V, −0.69 V, and −0.76 V for AuNPs/rGO-1, AuNPs/rGO-2, and AuNPs/rGO-3, respectively. The enhanced electrochemical response in the redox processes indicated the electroconducting properties of the AuNPs and rGO in facilitating the electron transfer between the electrode surface and phosphate buffer ions (curves a, b, and c) [29,30]. The increase in the electrochemical response suggested the high coverage coating of the AuNPs/rGO nanocomposite on the SPE. AuNPs/rGO-1 exhibited the highest electrochemical behavior among the AuNPs/rGO-modified SPEs, which can be attributed to the higher AuNPs:rGO ratio in the composite [31]. Meanwhile, the AuNPs-modified SPE showed a sharp reduction peak at −0.92 V. The high electrochemical response suggested that the AuNPs-modified SPE had a large effective surface area, which was almost similar to that of AuNPs/rGO-1. Because of its outstanding electrochemical response, AuNPs/rGO-1 was used in the characterizations thereafter.

CV of an electroactive species, $Fe(CN)_6^{3-/4-}$, is a valuable tool for testing the kinetic barrier of the interface. Therefore, CV measurements of the bare SPE and AuNPs/rGO-modified SPEs in a 0.1 M KCl solution containing 1.0 mM $Fe(CN)_6^{3-/4-}$ redox pair were carried out. The redox peaks in the CV results for the bare SPE, AuNPs/rGO-1, AuNPs/rGO-2, and AuNPs/rGO-3 in 1.0 mM of $Fe(CN)_6^{3-/4-}$ are shown in Fig. 4A. For the bare SPEs, a well-defined redox wave was seen, with a peak-to-peak separation (ΔE_p) of 110 mV at 60 mVs^{-1}, indicating a fast electron transfer reaction [32]. After modification with the AuNPs/rGO nanocomposite, there is a decrease in the peak-to-peak separation and increase in the peak current electron transfer for $Fe(CN)_6^{3-/4-}$, indicating that AuNPs/rGO nanocomposite increased the effective surface area, which will enhance the electron transfer between the analyte

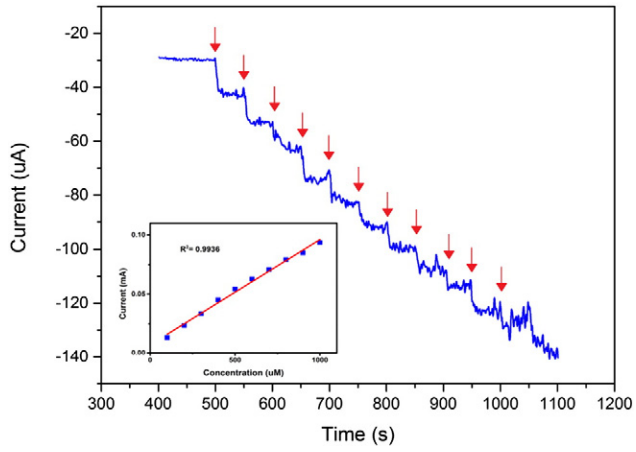

Fig. 7. Amperometry of AuNPs/rGO-1 in 0.1 M pH 7.4 PBS in the successive H_2O_2 concentration change of 100 μM. The potential was set at −0.5 V. Inset is the calibration curve of AuNPs/rGO-1 for the detection of H_2O_2.

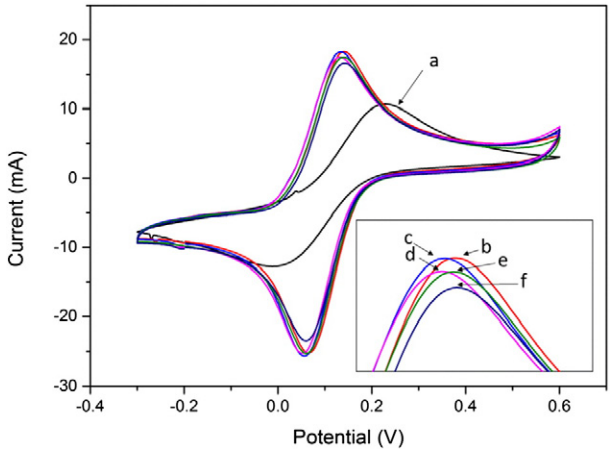

Fig. 9. Cyclic voltammogram of bare SPE (a), AuNPs/rGO-modified SPE (b) and AuNPs/rGO-modified SPE with stepwise immobilization of primary antibody (c), CEA (d), secondary antibody (e) and secondary antibody labeled HRP (f) in 0.1 M KCl solution containing 1.0 mM $Fe(CN)_6^{3-/4-}$. The scan rate was 60 mVs^{-1}.

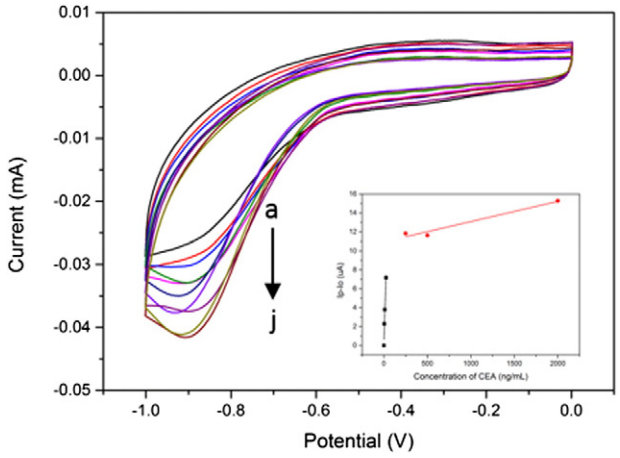

Fig. 10. Cyclic voltammatogram of immunosensor incubated with different concentration of CEA: 0.5 ng/mL (a), 5 ng/mL (b), 10 ng/mL (c), 25 ng/mL (d), 50 ng/mL (e), 100 ng/mL (f), 250 ng/mL (g), 500 ng/mL (h), 750 ng/mL (i) and 2000 ng/mL (j) and studied in 0.1 M PBS containing 0.5 μM H_2O_2. Inset is the calibration curve of immunosensor with varied concentration of CEA. Scan rate was 60 mVs^{-1}.

and electrode surface [33]. Fig. 4B shows a comparison of the redox peaks between the bare SPE, AuNPs/rGO-1, AuNPs-modified SPE, and rGO-modified SPE. It can be observed that after the modification with nanomaterials (AuNPs, rGO and both), the peak-to-peak separation of the redox peaks decreases, coupled with an increase in the peak current. The AuNPs-modified SPE shows a high peak current because AuNPs play a role in increasing the effective surface area of the electrode. The effective surface area of the modified SPEs was determined from a linear graph of the anodic and cathodic peak current (I_p) versus the square root of the scan rate [$v^{1/2}$] (Fig. 4C). By applying the Randles–Sevcik equation, the effective surface area of each SPE could be determined and tabulated in Table 1. The increase in the effective surface area of the SPEs suggested that the AuNPs and rGO were successfully deposited on the electrode surface.

The stability the AuNPs/rGO-modified SPEs was characterized using CV for 50 cycles in 0.1 M PBS. Fig. 5A, B, and C show that the three AuNPs/rGO-modified SPEs were relatively stable because the electrodes retained their initial electrochemical response after 50 cycles. The anodic peak that appeared at −0.6 V in Fig. 5A indicated a better electrochemical response for AuNPs/rGO-1 to the electrolyte and will be further characterized using H_2O_2 detection.

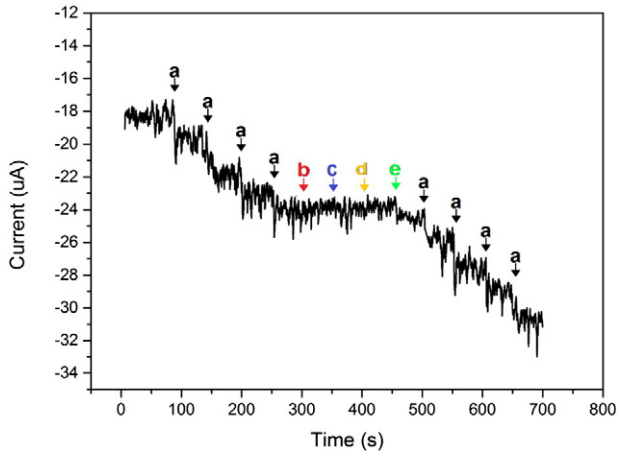

Fig. 11. Amperometric curve of immunosensor upon subsequent addition of 25 μM of H_2O_2 (a), 40 μM of glucose (b), 40 μM of urea (c), 40 μM of iron (III) acetate (d), and 40 μM of BSA (e) in 0.1-M PBS solution (pH 7.4). Applied potential was −0.5 V.

Table 1
Effective surface areas of bare SPE, AuNPs-modified SPE, rGO-modified SPE, and AuNPs/rGO-modified SPEs using $Fe(CN)_6^{3-/4-}$ as probe.

SPE	Effective surface area (cm^2)
Bare SPE	0.062
AuNPs/rGO-1	0.158
AuNPs/rGO-2	0.133
AuNPs/rGO-3	0.134
AuNPs-modified SPE	0.155
rGO-modified SPE	0.151

3.3. Detection capability of AuNPs/rGO modified SPE toward H_2O_2

Based on the characterization using blank PBS (Figs. 3 and 5) and $Fe(CN)_6^{3-/4-}$ redox probe (Fig. 4A), the optimized GO concentration for AuNPs/rGO nanocomposite was 0.1 mg/mL due to its prominent electrochemical properties and stability compared to those of 0.5 mg/mL and 1.0 mg/mL GO concentrations. The characterizations of the bare SPE and AuNPs/rGO-1 for the reduction of various H_2O_2 concentrations were carried out using CV, and the corresponding cyclic voltammogram is shown in Fig. 6. It can be observed that the reduction of H_2O_2 occurs at a fixed potential of −0.7 V, and the cathodic current increases with the concentration of H_2O_2 (curves a to h), showing the synergistic effect of the AuNPs and rGO nanocomposite in tunneling electron produced from reduction of H_2O_2 [34]. This result suggests the potential of the modified SPEs to be used as electrochemical sensors for the detection of H_2O_2, relative to the bare SPE (curve a′). From the calibration curve of AuNPs/rGO-1 (inset), it was confirmed that the AuNPs/rGO-modified SPE had a detection range of 20–800 μM ($R^2 = 0.9589$), and the limit of detection (LOD) was estimated to be 9.17 μM. A Tafel plot for the reduction of H_2O_2 by AuNPs/rGO-1 was also reported (Fig. S1A), in which the electron transfer coefficient (α) and standard heterogeneous electron transfer constant (k_s) were calculated to be 0.34 and 32.1 cms^{-1}, respectively.

Amperometry was performed to study the relationship between the concentration and reduction current. The amperometric characterization of AuNPs/rGO-1 was conducted in 0.1 M PBS (pH 7.4). Fig. 7 shows the amperometric response of AuNPs/rGO-1 upon consecutive H_2O_2 concentration changes of 100 μM. The amperometric current showed a linear response with the H_2O_2 concentration and a rapid respond time of 2 s, indicating fast electron transfer. The amperometry and the calibration curves of AuNPs-modified SPE (Fig. S2) and rGO-modified SPE (Fig. S3) were also reported. Plotting the calibration curve (inset) showed that AuNPs/rGO-1 had a regression equation: I(A) = 7E−06 + 0.0893 C (M) from 100 μM to 1000 μM ($R^2 = 0.9936$), and the limit of detection was estimated to be 29.8 μM with signal-to-noise ratio of 3 [35].

3.4. Immobilization of biomolecules on AuNPs/rGO-modified SPE

The electrochemical properties of AuNPs/rGO-1 and the immunosensor were studied using CV in 0.1-M PBS (pH 7.4) containing 5 μM of H_2O_2. Fig. 8 shows a reduction peak at −0.9 V, indicating the reduction current of H_2O_2 (curve a). Upon immobilization with a complete sandwich ELISA system, the reduction peak increased and shifted to a more positive potential (curve b). The higher peak current of the immunosensor in PBS containing 5 μM H_2O_2 was contributed by the electrocatalytic reduction of H_2O_2 by the HRP that was attached to the secondary antibody. Without the catalytic action of HRP, the peak current for the reduction of H_2O_2 was lower [36]. Additionally, the electron flow was facilitated by the high electroconductivity and increased surface area of AuNPs/rGO-modified electrode. The mechanism for reduction of H_2O_2 by HRP is depicted by Scheme 1.

To support the establishment of sandwich type immunoassay on the surface of AuNPs/rGO-modified SPE, each stage of immobilization was

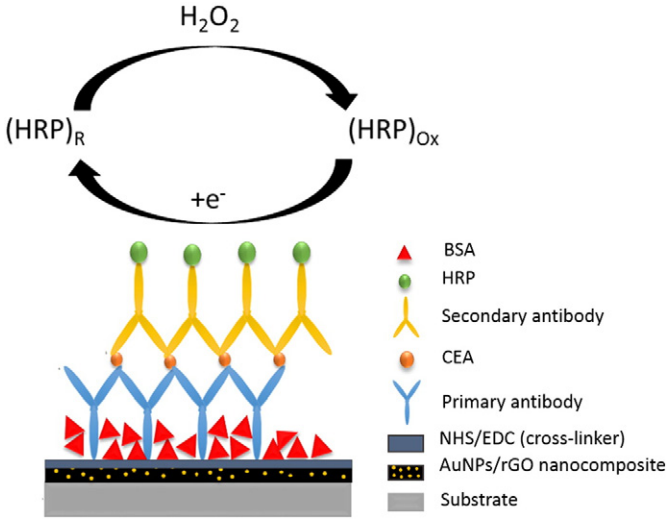

Scheme 1. Schematic of electrocatalytic reduction of H_2O_2 by the HRP attached on the immunoassay system.

characterized with CV in an $Fe(CN)_6^{3-/4-}$ redox probe. The cyclic voltammogram in Fig. 9 showed that the modification of AuNPs/rGO on a SPE increased the electron transfer kinetics as displayed by increased redox peaks. The immobilization with primary antibody decreased the redox peak current because the attachment of biomolecules on electrode surface inhibited the electron transfer. Similarly, stepwise immobilization of CEA, secondary antibody and secondary antibody-labeled HRP also inhibited the electron transfer and caused the peak current to decrease. The peak current reduction at each step indicated that the biomolecules were attached on top of the other to establish a sandwich immunoassay.

The detection capability of the immunosensor toward various concentrations of CEA was examined using CV in a 0.1 M PBS solution containing 5 μM of H_2O_2. Fig. 10 indicates that a reduction peak at −0.9 V increases with the CEA concentration (curves a to j). This could be explained by the increasing amount of conjugated antibody containing the HRP label immobilized in the sandwich system, which was completed as a result of the increasing amount of CEA present in the system [37]. Quantitatively, the immobilized HRP as the topmost layer of the system catalyzed the reduction of H_2O_2. From the calibration graph (inset), two linear detection ranges were plotted for various concentrations of CEA. At a lower linear range (0.5 to 25 ng/mL), the immunosensor had a detection limit of 0.28 ng/mL, while at a higher linear range (250 to 2000 ng/mL), the detection limit was 181.5 ng/mL. A Tafel plot based on the reduction of H_2O_2 by immunosensor was reported (Fig. S1B). The electron transfer coefficient (α) and standard heterogeneous electron transfer constant (k_s) of immunosensor were calculated as 0.128 and 21.9 cms^{-1}, respectively. In order to determine the catalytic rate constant (k_{cat}) of immunosensor, amperometry in blank PBS, and PBS containing 600 μM and 700 μM of H_2O_2 were conducted and the corresponding amperograms were plotted (Fig. S4). Based on the slope of I_c/I_L vs $t^{1/2}$ for the diffusion-controlled process (inset of Fig. S4), k_{cat} can be determined according to the Galus method (Eq. (1)) [38]. The value of k_{cat} was calculated to be 2.33×10^3 Ms^{-1}.

$$\frac{I_c}{I_L} = \pi^{\frac{1}{2}}(k_{cat}C_b)^{\frac{1}{2}} \quad (1)$$

where I_c is the catalytic current, I_L is the limited current in the absence of H_2O_2, and C_b is the bulk concentration of H_2O_2.

Table 2 lists examples of gold nanoparticle-based electrochemical biosensors for the detection of biomarkers, along with their limits of detection and approaches to the synthesis of active materials.

The selectivity of the immunosensor toward H_2O_2 among other interfering biomolecules was studied using amperometry in a 0.1 M PBS solution with subsequent additions of 25 μM of H_2O_2, 40 μM of glucose, 40 μM of urea, 40 μM of iron (III) acetate, and 40 μM of BSA. From Fig. 11, the addition of H_2O_2 showed a drop in

Table 2
Gold nanoparticle-based electrochemical biosensors for biomarkers and their linear ranges and limits of detection.

Method	Target biomarker	Approaches of synthesis of active materials	Linear range	Limit of detection	Reference
Au@Pd/Ag yolk–bimetallic shell nanoparticles and amination graphene using glassy carbon electrode	Nuclear matrix protein 22	Chemical reduction using sodium citrate	0.01–0.18 ng/mL	3.3 pg/mL	[39]
Bio-electrocatalytic reaction involving Au nanoparticles using micro-comb electrodes	Aflatoxin B_1	Chemical vapor deposition	0.5–10 ng/mL	0.1 ng/mL	[40]
Flow-injection immuno-bioassay with Au nanoparticles modified screen-printed electrodes	Interleukin-6	Electrochemical deposition	5–100 fg/mL	1.0 pg/mL	[41]
Ultrathin alumina sol–gel-derived films Au nanoparticles on gold electrode modified with a self-assembled mercaptoacetic acid (MAA) monolayer.	Transferrin	Chemical vapor deposition	1–75 ng/mL	0.05 ng/mL	[42]
Au-nanoparticle-and thionine modified carbon-paste electrode (CPE) interface	Cancer antigen 125 (CA125)	Electrochemical deposition	10–30 U/mL	1.8 U/mL *1 unit (U) is the amount of enzyme that catalyzes the reaction of 1 nmol of substrate per minute	[43]
Acetylcholinesterase biosensor based on 3-carboxyphenylboronic acid/reduced graphene oxide–gold nanocomposites modified electrode	Organophosphorus and carbamate pesticides	Deposition	0.1–150 ppb	0.1 ppb	[44]
New label free CA125 detection based on gold nanostructured screen-printed electrode	Cancer antigen 125 (CA125)	Electrodeposition	0–100 U/mL	6.7 U/mL	[4]
Self-assembly of 6 nm (diameter) colloidal Au onto the self-assembled monolayers (SAMs) of 4-aminothiophenol modified gold electrode	Hepatitis B	Adsorption	0.5–200 ng/mL	50 fg/mL	[31]
A novel hydrogen peroxide biosensor based on Au–graphene–HRP–chitosan biocomposites	Hydrogen peroxide (H_2O_2)	Adsorption	5 μM–5.13 mM	17 μM	[29]
Horseradish peroxidase functionalized nanocomposite as trace label	Carcinoembryonic antigen (CEA)	Chemical reduction	0.02–80.0 ng/mL	0.008 ng/mL	[45]
Electrochemical sensor for immunoassay of carcinoembryonic antigen based on thionine monolayer modified gold electrode	Carcinoembryonic antigen (CEA)	Adsorption	0.6–200 ng/mL	0.2 ng/mL	[46]
Immunosensor based on gold nanoparticles and graphene nanocomposites.	Carcinoembryonic antigen (CEA)	Electrodeposition	0.5–25 ng/mL 250–2000 ng/mL	0.28 ng/mL 181.5 ng/mL	This work.

current, which was due to the reduction of H_2O_2 by the immobilized HRP. In contrast, the additions of the glucose, urea, and iron (III) acetate did not cause any drop in current, and the addition of BSA showed an insignificant reduction in current. Therefore, the immunosensor exhibited an unambiguous response toward the reduction of H_2O_2 and was highly selective as an immunosensor.

4. Conclusion

An immunosensor for the detection of CEA based on an AuNPs/rGO-modified SPE was successfully fabricated by the in-situ electrodeposition of rGO nanocomposites and the reduction of AuNPs on a carbon SPE. Characterizations proved that the modified SPE exhibited a larger effective surface area, higher electron transfer kinetics and high stability toward the electrocatalytic reduction of H_2O_2. The amperometric current increased linearly when increasing the H_2O_2 concentration in the range of 100–1000 μM, and the lowest detection limit was estimated to be 29.8 μM. The modified SPE was also compatible with the sandwich ELISA system and was highly sensitive toward the presence of CEA. Hence, the immunosensor has significant potential for sensing CEA.

Acknowledgments

This research was supported by a Fundamental Research Grant Scheme (FRGS/1/2012/ST05/UPM/02/3) and a High Impact Research Grant (UM.C/625/1/HIR/MOHE/SC/21) from the Ministry of Higher Education of Malaysia.

Appendix A. Supplementary data

Supplementary data to this article can be found online at http://dx.doi.org/10.1016/j.msec.2015.09.010.

References

[1] U. Eswaran, Sreelakshmi, V. Eswaran, Embedded system based automated drug delivery unit and microfluidics for drug discovery, Cancer 1 (1) (2012).
[2] Y.-E. Choi, J.-W. Kwak, J.W. Park, Nanotechnology for early cancer detection, Sensors 10 (1) (2010) 428–455.
[3] H. Chen, C. Jiang, C. Yu, S. Zhang, B. Liu, J. Kong, Protein chips and nanomaterials for application in tumor marker immunoassays, Biosens. Bioelectron. 24 (12) (2009) 3399–3411.
[4] A. Ravalli, G. Pilon dos Santos, M. Ferroni, G. Faglia, H. Yamanaka, G. Marrazza, New label free CA125 detection based on gold nanostructured screen-printed electrode, Sensors Actuators B Chem. 179 (2013) 194–200.
[5] N. Bojorge Ramírez, A.M. Salgado, B. Valdman, The evolution and developments of immunosensors for health and environmental monitoring: problems and perspectives, Braz. J. Chem. Eng. 26 (2) (2009) 227–249.
[6] S. Zhang, X. Li, F. Zhang, CE-based simultaneous liquid-phase noncompetitive enzyme immunoassay for three tumor markers in human serum using electrochemical detection, Electrophoresis 28 (23) (2007) 4427–4434.
[7] J. Wang, Electrochemical nucleic acid biosensors, Anal. Chim. Acta 469 (1) (2002) 63–71.
[8] M.L. Sin, K.E. Mach, P.K. Wong, J.C. Liao, Advances and challenges in biosensor-based diagnosis of infectious diseases, Expert. Rev. Mol. Diagn. 14 (2) (2014) 225–244.
[9] J. Wang, Electrochemical biosensors: towards point-of-care cancer diagnostics, Biosens. Bioelectron. 21 (10) (2006) 1887–1892.
[10] J.-I. Kim, A. Bordeanu, J.-C. Pyun, Diamond-like carbon (DLC) microelectrode for electrochemical ELISA, Biosens. Bioelectron. 24 (5) (2009) 1394–1398.
[11] S. Numthuam, T. Kakegawa, T. Anada, A. Khademhosseini, H. Suzuki, J. Fukuda, Synergistic effects of micro/nano modifications on electrodes for microfluidic electrochemical ELISA, Sensors Actuators B Chem. 156 (2) (2011) 637–644.
[12] T. Tangkuaram, C. Ponchio, T. Kangkasomboon, P. Katikawong, W. Veerasai, Design and development of a highly stable hydrogen peroxide biosensor on screen printed carbon electrode based on horseradish peroxidase bound with gold nanoparticles in the matrix of chitosan, Biosens. Bioelectron. 22 (9–10) (2007) 2071–2078.
[13] S.-I. Wei, Design and implementation of an all solid-state multi-ions sensing system based on LabVIEW software technology, Electron. Eng. (2006).
[14] O. Domínguez-Renedo, M.A. Alonso-Lomillo, M.J. Arcos-Martínez, Disposable electrochemical biosensors in microbiology, Talanta 73 (2007) 202–219.
[15] W. Siangproh, W. Dungchai, P. Rattanarat, O. Chailapakul, Nanoparticle-based electrochemical detection in conventional and miniaturized systems and their bioanalytical applications: a review, Anal. Chim. Acta 690 (1) (2011) 10–25.
[16] E. Er, H. Çelikkan, N. Erk, M. Levent Aksu, A new generation electrochemical sensor based on graphene nanosheets/gold nanoparticles/nafion nanocomposite for determination of silodosin, Electrochim. Acta 157 (2015) 252–257.
[17] P. Sharma, G. Darabdhara, T.M. Reddy, A. Borah, P. Bezboruah, P. Gogoi, N. Hussain, P. Sengupta, M.R. Das, Synthesis, characterization and catalytic application of Au NPs–reduced graphene oxide composites material: an eco-friendly approach, Catal. Commun. 40 (2013) 139–144.
[18] K. Kerman, M. Saito, E. Tamiya, S. Yamamura, Y. Takamura, Nanomaterial-based electrochemical biosensors for medical applications, TrAC Trends Anal. Chem. 27 (7) (2008) 585–592.
[19] M.A. Tabrizi, A. Tavakkoli, V. Dhand, K.Y. Rhee, S.-J. Park, Eco-friendly one-pot synthesis of gold decorated reduced graphene oxide using beer as a reducing agent, J. Ind. Eng. Chem. 20 (6) (2014) 4327–4331.
[20] N.M. Huang, H.N. Lim, C.H. Chia, M.A. Yarmo, M.R. Muhamad, Simple room-temperature preparation of high-yield large-area graphene oxide, Int. J. Nanomedicine 6 (2011) 3443.
[21] A. Jamil, H.N. Lim, N.A. Yusof, A. Ahmad Tajudin, N.M. Huang, A. Pandikumar, A. Moradi Golsheikh, Y.H. Lee, Y. Andou, Preparation and characterization of silver nanoparticles–reduced graphene oxide on ITO for immunosensing platform, Sensors Actuators B Chem. (2015).
[22] Y. Hu, J. Jin, P. Wu, H. Zhang, C. Cai, Graphene–gold nanostructure composites fabricated by electrodeposition and their electrocatalytic activity toward the oxygen reduction and glucose oxidation, Electrochim. Acta 56 (1) (2010) 491–500.
[23] M. Amal Raj, S. Abraham John, Assembly of gold nanoparticles on graphene film via electroless deposition: spontaneous reduction of Au^{3+} ions by graphene film, RSC Adv. 5 (7) (2015) 4964–4971.
[24] K.S. Subrahmanyam, A.K. Manna, S.K. Pati, C.N.R. Rao, A study of graphene decorated with metal nanoparticles, Chem. Phys. Lett. 497 (1–3) (2010) 70–75.
[25] S.C. Jun, Fundamental of graphene, Graphene-based Energy Devices 2015, pp. 1–48.
[26] S.R. Sahu, M.M. Devi, P. Mukherjee, P. Sen, K. Biswas, Optical property characterization of novel graphene–X (X = Ag, Au and Cu) nanoparticle hybrids, J. Nanomater. 2013 (2013) 6.
[27] M.A. Tabrizi, J.N. Varkani, Green synthesis of reduced graphene oxide decorated with gold nanoparticles and its glucose sensing application, Sensors Actuators B Chem. 202 (2014) 475–482.
[28] Z. Luo, T. Yu, K.-j. Kim, Z. Ni, Y. You, S. Lim, Z. Shen, S. Wang, J. Lin, Thickness-dependent reversible hydrogenation of graphene layers, ACS Nano 3 (7) (2009) 1781–1788.
[29] K. Zhou, Y. Zhu, X. Yang, J. Luo, C. Li, S. Luan, A novel hydrogen peroxide biosensor based on Au–graphene–HRP–chitosan biocomposites, Electrochim. Acta 55 (9) (2010) 3055–3060.
[30] J. Han, Y. Zhuo, Y.-Q. Chai, L. Mao, Y.-L. Yuan, R. Yuan, Highly conducting gold nanoparticles–graphene nanohybrid films for ultrasensitive detection of carcinoembryonic antigen, Talanta 85 (1) (2011) 130–135.
[31] M. Wang, L. Wang, G. Wang, X. Ji, Y. Bai, T. Li, S. Gong, J. Li, Application of impedance spectroscopy for monitoring colloid Au-enhanced antibody immobilization and antibody–antigen reactions, Biosens. Bioelectron. 19 (6) (2004) 575–582.
[32] S. Sabury, S.H. Kazemi, F. Sharif, Graphene–gold nanoparticle composite: application as a good scaffold for construction of glucose oxidase biosensor, Mater. Sci. Eng. C 49 (2015) 297–304.
[33] X. Sun, M. Jia, L. Guan, J. Ji, Y. Zhang, L. Tang, Z. Li, Multilayer graphene–gold nanocomposite modified stem-loop DNA biosensor for peanut allergen-Ara h1 detection, Food Chem. 172 (2015) 335–342.
[34] C. Shan, H. Yang, D. Han, Q. Zhang, A. Ivaska, L. Niu, Graphene/AuNPs/chitosan nanocomposites film for glucose biosensing, Biosens. Bioelectron. 25 (5) (2010) 1070–1074.
[35] S. Jayabal, P. Viswanathan, R. Ramaraj, Reduced graphene oxide–gold nanorod composite material stabilized in silicate sol–gel matrix for nitric oxide sensor, RSC Adv. 4 (63) (2014) 33541–33548.
[36] Z. Zhong, W. Wu, W. Dong, D. Wang, J. Shan, Y. Qing, Z. Zhang, Nanogold-enwrapped graphene nanocomposites as trace labels for sensitivity enhancement of electrochemical immunosensors in clinical immunoassays: carcinoembryonic antigen as a model, Biosens. Bioelectron. 25 (10) (2010) 2379–2383.
[37] H. Chen, D. Tang, B. Zhang, B. Liu, Y. Cui, G. Chen, Electrochemical immunosensor for carcinoembryonic antigen based on nanosilver-coated magnetic beads and gold–graphene nanolabels, Talanta 91 (2012) 95–102.
[38] A.A. Ensafi, H. Karimi-Maleh, S. Mallakpour, B. Rezaei, Highly sensitive voltammetric sensor based on catechol-derivative-multiwall carbon nanotubes for the catalytic determination of captopril in patient human urine samples, Colloids Surf. B: Biointerfaces 87 (2) (2011) 480–488.
[39] N. Li, Y. Wang, Y. Li, W. Cao, H. Ma, D. Wu, D. Bin, Q. Wei, A label-free electrochemical immunosensor based on Au@Pd/Ag yolk–bimetallic shell nanoparticles and amination graphene for detection of nuclear matrix protein 22, Sensors Actuators B Chem. 202 (2014) 67–73.
[40] Y. Liu, Z. Qin, X. Wu, H. Jiang, Immune-biosensor for aflatoxin B1 based bioelectrocatalytic reaction on micro-comb electrode, Biochem. Eng. J. 32 (3) (2006) 211–217.
[41] K.Z. Liang, W.J. Mu, Flow-injection immuno-bioassay for interleukin-6 in humans based on gold nanoparticles modified screen-printed graphite electrodes, Anal. Chim. Acta 580 (2) (2006) 128–135.
[42] T. Yin, W. Wei, L. Yang, X. Gao, Y. Gao, A novel capacitive immunosensor for transferrin detection based on ultrathin alumina sol–gel-derived films and gold nanoparticles, Sensors Actuators B Chem. 117 (1) (2006) 286–294.

[43] D. Tang, R. Yuan, Y. Chai, Electrochemical immuno-bioanalysis for carcinoma antigen 125 based on thionine and gold nanoparticles-modified carbon paste interface, Anal. Chim. Acta 564 (2) (2006) 158–165.
[44] T. Liu, S. Haichao, Q. Xiangjin, J. Peng, C. Lin, S. Ai, Acetylcholinesterase biosensor based on 3-carboxyphenylboronic acid/reduced graphene oxide–gold nanocomposites modified electrode for amperometric detection of organophosphorus and carbamate pesticides, Sensors Actuators B Chem. 160 (1) (2011) 1255–1261.
[45] D. Feng, L. Li, X. Fang, X. Han, Y. Zhang, Dual signal amplification of horseradish peroxidase functionalized nanocomposite as trace label for the electrochemical detection of carcinoembryonic antigen, Electrochim. Acta 127 (2014) 334–341.
[46] Z. Dai, J. Chen, F. Yan, H. Ju, Electrochemical sensor for immunoassay of carcinoembryonic antigen based on thionine monolayer modified gold electrode, Cancer Detect. Prev. 29 (3) (2005) 233–240.